UNIVERSITY *of* York

This is a repository copy of *Normal modes and mode transformation of pure electron vortex beams*.

White Rose Research Online URL for this paper:
https://eprints.whiterose.ac.uk/id/eprint/112543/

Version: Published Version

Article:

White Rose
university consortium
Universities of Leeds, Sheffield & York

eprints@whiterose.ac.uk
https://eprints.whiterose.ac.uk/

Research

Author for correspondence:
J. Yuan
e-mail: jun.yuan@york.ac.uk

Normal modes and mode transformation of pure electron vortex beams

G. Thirunavukkarasu, M. Mousley, M. Babiker and J. Yuan

Department of Physics, University of York, Heslington, York YO10 5DD, UK

JY, 0000-0001-5833-4570

Electron vortex beams constitute the first class of matter vortex beams which are currently routinely produced in the laboratory. Here, we briefly review the progress of this nascent field and put forward a natural quantum basis set which we show is suitable for the description of electron vortex beams. The normal modes are truncated Bessel beams (TBBs) defined in the aperture plane or the Fourier transform of the transverse structure of the TBBs (FT-TBBs) in the focal plane of a lens with the said aperture. As these modes are eigenfunctions of the axial orbital angular momentum operator, they can provide a complete description of the two-dimensional transverse distribution of the wave function of any electron vortex beam in such a system, in analogy with the prominent role Laguerre–Gaussian (LG) beams played in the description of optical vortex beams. The characteristics of the normal modes of TBBs and FT-TBBs are described, including the quantized orbital angular momentum (in terms of the winding number l) and the radial index $p > 0$. We present the experimental realization of such beams using computer-generated holograms. The mode analysis can be carried out using astigmatic transformation optics, demonstrating close analogy with the astigmatic mode transformation between LG and Hermite–Gaussian beams.

This article is part of the themed issue 'Optical orbital angular momentum'.

THE ROYAL SOCIETY
PUBLISHING

1. Introduction

The ground-breaking work by Allen *et al.* [1] was indeed a profound development which led physicists to a new understanding of the physics of light. The main premise of the work reported in 1992 was that light modes can be generated, endowed with the property of quantized orbital angular momentum (OAM). As a concept, OAM was in fact discussed earlier by several authors, including Belinfante [2] and Humblet [3]. A more recent suggestion about modes with vortex characteristics analogous to superfluid vortices by Coullet *et al.* [4] did not recognize the significance of the quantization of the OAM of light and the possibility of their generation as constituting a major breakthrough. Research on light carrying OAM swiftly followed the paper by Allen *et al.* [1] and continued apace over the last quarter of a century, leading not only to fundamental developments in the field of optics but also to a number of significant applications [5–7]. These include the optical spanner as the rotational equivalent of optical tweezers which has been involved in various applications [8–11]. Further developments include micromanipulation [12], quantum communications [13], phase contrast imaging [14–16] and proposals for applications in metrology and quantum information.

One of the significant developments that has emerged recently as a direct consequence of the research on the OAM of light is the realization that this new beam property is not the preserve of optical beams alone, but can be extended to apply to any matter (de Broglie) wave. Electrons as the prototypical example of a de Broglie wave came to the fore as the first candidate for a matter vortex beam. Although suggestions for particle vortex beams were made first by Bialynicki-Birula *et al.* [17–19], the main thrust of research specifically on electron vortex beams is due to the work by Bliokh *et al.* [20] and electron vortices were then experimentally realized in earlier studies [21–23] inside electron microscopes from 2010 onwards. The main technique for the realization of electron vortex beams includes computer-generated holographic masks applied in similar ways to those routinely adopted in the creation of optical vortex beams [24,25]. Other techniques include spiral phase plates [21,26], proposed spin–orbit angular momentum converters [27] and a method which relies on the Aharonov–Bohm effect [28,29]. More recently, such beams have also been generated using electron sieves [30].

With optical vortex beams as the first member, electron vortex beams are now regarded as the second member of a class of freely propagating vortex states. There are recent studies on neutron vortex beams [31] and suggestions for atom vortex beams [32]. Further developments of neutron and atom vortex beams are certainly desirable for diverse applications not least in the context of the foundations of quantum mechanics and quantum information, but for possible new forms of interactions of such beams with matter. However, the realization of proper vortex beams of these types appears to be rather challenging at present as they would require coherent sources as a first step, which are still to be developed.

A vortex beam, in general, can be defined as a wave of freely propagating particles characterized by a wavefront whose topological structure stems from a phase factor $e^{il\phi}$ in the associated wave function, with ϕ the azimuthal angle and l the topological charge (or winding number). Topological wavefronts were first recognized by Nye & Berry [33] as dislocations in wave trains in a manner reminiscent of that for crystal defects. The OAM associated with this phase is of magnitude $l\hbar$ per particle and depends only on the topological charge l, which is an integer and can take both positive and negative values. Allen *et al.* [1] recognized that laser lights with a Laguerre–Gaussian (LG) amplitude distribution are optical vortex beams with well-defined OAM. Besides the topological charge l, the LG beam (LG_{pl}) for which the wave function is $\Psi_p^l(\rho, \phi, z)$ depends also on the radial index $p \geq 0$, which specifies the radial variation of the amplitude function; there are $p + 1$ nodes in the radial intensity distribution. Index p has so far featured little in both experimental and theoretical analyses of vortex beams that seemed to have concentrated primarily on the cases where $p = 0$, in which the modes are called doughnut modes. This has led some to refer to the p index as the forgotten quantum number in optical vortex beam physics [34]. Similarly, the radial structure has not yet featured much in research on electron vortex beams [35].

3

rsta.royalsocietypublishing.org *Phil. Trans. R. Soc. A* **375**: 20150438

Although much of electron vortex research is inspired by concepts and techniques in optical vortex beams, due to the equivalence of scalar Maxwell equations in free space and the Schrödinger equation for a free particle [17–20], electron vortex beams are characterized by a number of different properties [20]. These are attributable to the fact that electrons have finite mass, carry electric charge and have half-integer intrinsic angular momentum (spin). Furthermore, there are considerable differences in scale. Electron vortex beams created inside contemporary electron microscopes have de Broglie wavelengths in the picometre range and are therefore capable of probing much smaller features than is possible using optical vortex beams for which the typical wavelength is in the hundreds of nanometres range (visible light). In X-ray microscopy, the lack of efficient focusing devices also limits the practical resolution of an emergent X-ray vortex beam to be as useful as an electron vortex beam for the purpose of resolving atomic structure. In addition, the production of optical vortex beams has benefited from the availability of highly collimated laser beams. The laser cavity modes naturally give rise to the transverse amplitude distribution in Hermite–Gaussian (HG) modes with spatial dependence $HG_{mn} = H_m(x)H_n(y)G(x,y)$, where H_m is the Hermite polynomial of order m and G stands for Gaussian envelope function. The LG optical vortex beams can be generated from HG non-vortex beams by a mode converter involving cylindrical lenses [36]. By comparison, electron beams of usable currents are typically only partially coherent. To improve the coherence, only a small part of the transverse area of the wavefront can be selected using apertures to form the electron vortex beams. This means that the LG basis set (LG_{pl}) discussed in [1] may not be a suitable natural quantum basis for electron vortex beams. In this report, we put forward a different basis set in the form of truncated Bessel beams (TBBs) in the aperture plane and show how they form a more natural quantum basis for electron vortex beams.

Electron vortex research promises applications in a number of contexts, including microscopical analysis, where the OAM of the beam is expected to provide useful new information about the crystallographic, electronic and magnetic properties of materials. Indeed electron diffraction has already exhibited signs of chirality [37] as well as information about the magnetic properties as revealed in electron energy-loss spectroscopy (EELS) [22]. Although confirmation for the latter is still lacking, the physical principles of OAM transfer have proven to be valid in the strong dipole excitation [38], but caution is required as to the effect of the location of the atoms relative to the beam axis [39] and dynamical scattering [40] further complicates the picture of the OAM transfer involved. If high spatial resolution is achievable in electron microscopy, it would facilitate the mapping of magnetic information at the atomic scale. Additionally, the inherent phase structure of the vortex is considered ideal for applications in high-resolution phase contrast imaging, as required for biological specimens with low absorption contrast [41]. Electron vortex beams may find application in the manipulation of nanoparticles [42–44], as in electron spanners where the vortex beam imparts a torque on a nanoparticle in analogy with optical spanners [45]. Electron vortex states are also relevant in the context of quantum information and, in particular, the electron vortex may potentially be used to impart angular momentum into vortices in Bose–Einstein condensates [46]. The OAM and magnetic properties of the electron vortex may also find potential uses in spintronic applications, either in the characterization of spintronic devices or in contexts employing spin-polarized current injection, through spin-to-orbital angular momentum conversion processes [27,47].

As mentioned earlier, the transverse, in-plane, radial structure of electron vortex beams has not received much attention, with work concentrating so far mainly on doughnut-type modes which display only azimuthal dependence in ring-like intensity distributions. This means that the transverse structure of the vortex beam is not completely defined, as both azimuthal and radial quantum numbers are necessary to represent the two degrees of freedom in the transverse plane of a paraxial electron beam. In vortex beam research, the emphasis has been rightly focused on the characteristic azimuthal phase dependence $e^{il\phi}$. However, the radial mode dependence can be used in quantum manipulation and for encoding information for quantum communication and computing [48]. Here, we present the orthonormal TBB set of modes, characterized by radial and azimuthal quantum numbers p and l, respectively, as a natural quantum basis for the

description of the transverse structure of the apertured wavefront of electron vortex beams or their Fourier transform (FT-TBBs), which can be found as the transverse structure of the amplitude distribution of the electron vortex beams at the focal plane of a lens placed in front of the apertured electron vortex beams. We demonstrate the production of the normal modes of electron vortex beams based on FT-TBBs possessing both well-defined azimuthal index l and radial index p. We show that the transverse structures of the FT-TBB vortex modes can be transformed by an astigmator lens to non-vortex beams in a manner similar to the transformation of LG modes to the HG modes as discussed by Allen *et al.* [1] and Abramochkin & Volostnikov [49]. As we argue here, we anticipate that in the context of electron vortices our results pave the way towards the complete control of the quantum state of matter vortex beams. This could provide the basis for the quantum manipulation of electron vortex beams, with potential applications in various quantum technologies such as quantum imaging or quantum information processing and in possible super-resolution microscopy.

2. Truncated Bessel beams and their Fourier transforms

As an electron vortex beam is typically produced from a partially coherent electron source, an aperture is used to capture the useful part of the wavefront (whose size is of the order of a spatial coherence length or less) in order to reduce the effect of the finite source size. Apertures are also used to limit the aberration of the electron optical system. This naturally suggests a set of TBBs, with wave functions given by $u_{pl}(\rho, \phi, z)$ in cylindrical polar coordinates, as a suitable quantum basis of the electron vortex beams at the aperture plane:

$$u_{pl}(\rho, \phi, z) = N_{pl} \exp{(ik_z z)} \exp{(il\phi)} J_l(k_\perp^{pl}\rho) \quad \text{for } \rho \le R, \tag{2.1}$$

where we have adopted the radial and azimuthal mode indices p and l, respectively, following the convention used for the LG modes [1]. In that case, J_l is the Bessel function of the first kind of order l, $k_\perp^{pl} = \lambda_{pl}/R$, with λ_{pl} the $(p + 1)$th zero of the lth-order Bessel function J_l, and R is the radius of the aperture. The azimuthal phase factor $\exp{(il\phi)}$ ensures that these modes are eigenfunctions of the axial OAM operator with quantized eigenvalues $l\hbar$. As a result, the truncated Bessel functions, together with the azimuthal phase factor, form a complete two-dimensional basis set of the OAM modes at the aperture plane.

Making use of the following identity:

$$\int_0^R J_l(k_\perp^{pl}\rho) J_l(k_\perp^{p'l}\rho)\rho \, d\rho = \frac{\delta_{p,p'}}{2} \left[J_{l+1}\left(\lambda_{pl}\right)\right]^2 \tag{2.2}$$

and the standard result

$$\int_0^{2\pi} \exp{(il\phi)} \exp{(-il'\phi)} \, d\phi = 2\pi \delta_{ll'} \tag{2.3}$$

the normalization factor N_{pl} can be shown to be $1/\sqrt{2}\,\pi J_{l+1}(\lambda_{pl})$, when the delta function normalization of the free-particle wave function in the z-direction is taken into account.

Now any arbitrary transverse amplitude distribution of an electron vortex beam defined at the aperture plane (ρ, ϕ, z) (as in figure 1) can be described as a linear combination of this set of basis functions:

$$\Phi(\rho, \phi, z) = \sum_p c_{pl} u_{pl}(\rho, \phi, z), \tag{2.4}$$

where the c_{pl}'s are the expansion coefficients. Such coefficients have been numerically evaluated for the electron vortex beam generated using a spiral-shaped phase plate [50].

More commonly, the aperture truncated electron vortex beam is focused by a lens to form an intense vortex beam. The amplitude distribution of such a vortex beam at the focal plane (q, θ, z) of the lens emerges in terms of the in-plane Fourier transform of the TBB wave function shown in equation (2.4). We can write

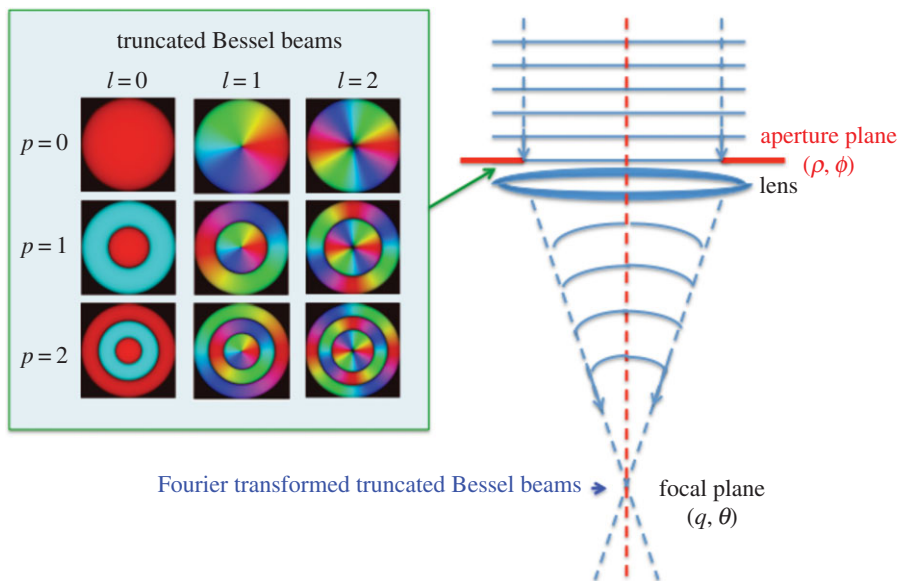$$\Psi(q, \theta, z) = \sum_p c_{pl} v_{pl}(q, \theta, z), \tag{2.5}$$

Figure 1. The electron vortex beam is produced by illuminating a phase mask with a plane wave and the resultant phase structured wave is focused using a lens to produce a focused vortex beam. The natural vortex beam eigenstates are travelling waves with a transverse structure described by a truncated Bessel function (shown in the inset), defined in Fourier space. The amplitude is represented by brightness and the phase by pseudo-colour spectrum between 0 and 2π, as illustrated by the linear azimuthal phase ramp for the $p = 0$ and $l = 1$ TBB mode.

where the FT-TBB mode function $v_{pl}(q, \theta, z)$ is the in-plane Fourier transform of the truncated Bessel beam mode function as given in (2.1)

$$v_{pl}(q, \theta, z) = \mathcal{FT}[u_{pl}(\rho, \phi, z)]. \tag{2.6}$$

Together with the azimuthal factor, it can be shown that the Fourier transform of the truncated Bessel functions also constitute a complete orthonormal quantum basis set with well-defined OAM. It is therefore ideal for the description of focused electron vortex beams.

It is instructive to examine the in-plane Fourier transform of the finite (truncated) Bessel beam mode function more closely. We have

$$v_{pl}(q, \theta, z) = \int_0^{2\pi} d\phi \int_0^R \rho \, d\rho N_{pl} J_l(k_\perp^{pl} \rho) e^{il\phi} e^{iq \cdot \rho}. \tag{2.7}$$

Making use of the Jacobi–Anger relationship

$$e^{iq \cdot \rho} = \sum_{n'=-\infty}^{\infty} i^{n'} J_{n'}(q\rho) e^{in'(\phi-\theta)}, \tag{2.8}$$

where ϕ and θ are the azimuthal angles for the in-plane vectors ρ and q, respectively, we have on substitution in equation (2.7)

$$v_{pl}(q, \theta, z) = \int_0^{2\pi} d\phi \int_0^R N_{pl} J_l(k_\perp^{pl} \rho) e^{il\phi} \left[\sum_{l'=-\infty}^{\infty} i^{l'} J_{l'}(q\rho) e^{il'(\phi-\theta)} \right] \rho \, d\rho. \tag{2.9}$$

Integration over the angular variable ϕ can now be done using equation (2.3). Thus, we find

$$v_{pl}(q, \theta, z) = N_{pl} i^l e^{il\theta} \int_0^R J_l(k_\perp^{pl} \rho) J_l(q\rho) \rho \, d\rho. \tag{2.10}$$

Finally, we make use of the following Bessel function identity:

$$\int_0^a J_m(k_1 r) J_m(k_2 r) r \, \mathrm{d}r = \frac{a}{k_1^2 - k_2^2} [k_2 J_m(k_1 a) J'_m(k_2 a) - k_1 J_m(k_2 a) J'_m(k_1 a)], \tag{2.11}$$

which leads to the result for the FT-TBB mode in the form:

$$v_{pl}(q, \theta, z) = \mathrm{i}^l N_{pl} R \, \mathrm{e}^{\mathrm{i}l\theta} \frac{[q J_l(k_\perp^{pl} R) J'_l(qR) - k_\perp^{pl} J_l(qR) J'_l(k_\perp^{pl} R)]}{k_\perp^{pl2} - q^2}. \tag{2.12}$$

The boundary conditions are such that the wave function vanishes at R. We have

$$J_l(k_\perp^{pl} R) = J_l(\lambda_{pl}) = 0, \tag{2.13}$$

where λ_{pl} is the $(p+1)$th zero of the Bessel function of the first kind of order l. The expression for v_{pl} simplifies accordingly

$$v_{pl}(q, \theta, z) = -\mathrm{i}^l \lambda_{pl} J'_l(\lambda_{pl}) \, \mathrm{e}^{\mathrm{i}l\theta} \frac{J_l(qR)}{k_\perp^{pl2} - q^2}. \tag{2.14}$$

Alternatively, we can make use of another identity of Bessel functions, namely

$$J'_l(x) = \tfrac{1}{2}[J_{l-1}(x) - J_{l+1}(x)], \tag{2.15}$$

to obtain

$$v_{pl}(q, \theta, z) = -\mathrm{i}^l \lambda_{pl} \, \mathrm{e}^{\mathrm{i}l\theta} \frac{J_l(qR)}{\sqrt{2}(k_\perp^{pl2} - q^2)} [J_{l-1}(\lambda_{pl}) - J_{l+1}(\lambda_{pl})]. \tag{2.16}$$

We emphasize that this FT-TBB mode is indeed a vortex beam with a well-defined OAM $l\hbar$ and a radial index p-dependent transverse distribution. It is easy to show that the FT-TBBs form another good quantum basis set for the description of electron vortex beams at the focal plane of a lens. The amplitude and phase of the first three p-modes of the $l = 1$ FT-TBB modes are shown in columns 2 and 3 in figure 2, respectively. These results show that the higher order radial modes are distinguished by $p + 1$ bright rings, reminiscent of the corresponding LG modes. However, the similarity does not extend to the additional faint ring structures that can be seen in the amplitude distribution of the FT-TBB$_{2,1}$ mode, with $p = 2$ and $l = 1$. These small ringed structures are caused by the ringing effect of the sharply defined aperture. Another notable feature is that the largest amplitude occurs when q approaches $k_\perp^{pl}$, in which case the wave function locally becomes a sinc function of the radial coordinate.

One way to understand the transverse distribution of the focused vortex beam shown in figure 2 is to compare with the LG modes as given by Allen et al. [1]. Similar to the LG modes, the number of bright ringed structures of our electron vortex normal modes increase with higher radial order vortex beams (increasing p). In LG modes with $p \geq 0$, the intensity cross section consists of $p + 1$ concentric rings with a zero on-axis intensity. In our FT-TBB normal modes, there are additional faint rings which can be shown to be related to the sharp cut-off of the circular aperture of the truncated Bessel functions. This can also be understood by regarding the original apertured mask as the product of the unobstructed Bessel beam and a top-hat mask function (see equation (2.16)). Then the transverse distribution of the vortex beam at the focal plane can be considered as the convolution of the Fourier transform of the Bessel function (where the transverse intensity is a ring with a radius controlled by the radial size of the first dark zone in the mask) and that of the top-hat mask (which is the well-known Airy pattern with side band ring features). This is consistent with the mathematical form of the Fourier transform of the normal modes in the aperture plane (see equation (2.16) and figure 2). As p increases, the size of the first-node ring shrinks and the Bessel ring at the focal plane increases in size. This explains the size changes of the brightest rings seen in figure 2 (middle column) for different values of p. This reciprocal relationship is consistent with the expectation based on the quantum uncertainty principle. The convolution of the Bessel rings with the Airy functions results in side bands, but they preserve the circular symmetry of the main Bessel rings.
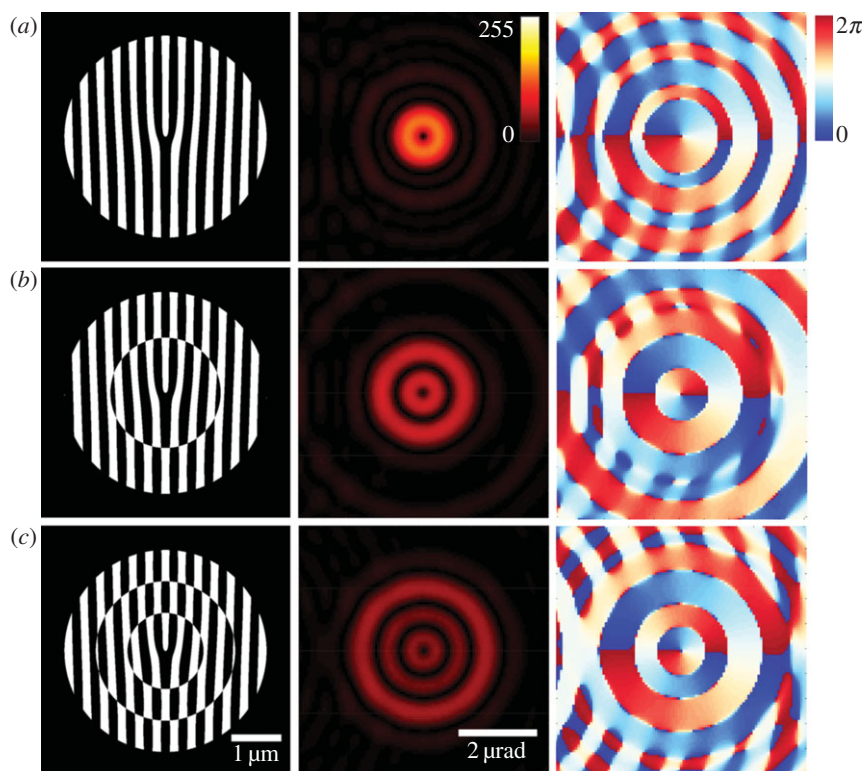
Figure 2. Computer-simulated diffractive holograms (left column) and intensity (middle column) and phase (right column) profiles for the vortex beam at the focal plane of the lens, with $l = 1$ but with different radial modes (a) $p = 0$, (b) $p = 1$ and (c) $p = 2$. The calculation is for 200 kV electrons (de Broglie wavelength $= 2.5$ pm).

3. Experimental production of the Fourier transform-truncated Bessel beam modes and their transformation

Both TBB and FT-TBB modes can be easily generated using the existing electron vortex beam technology. Here, we demonstrate that for the FT-TBB modes using a computer-generated hologram approach. The procedure for the experimental realization of the FT-TBB vortex modes is achieved by interfering a TBB mode with a plane wave to form a computer-generated hologram for use as an aperture for the vortex beam-forming lens. Examples of the design of the masks are shown in figure 2, together with the amplitude and phase structure of the resulting first-order diffracting beam.

The design of the computer-generated hologram is implemented on an Si_3N_4 membrane of 200 nm thickness whose top-flat-side is sputter coated with 50 nm thick $Pt_{80}Pd_{20}$ films to block the electron beam incident in regions other than the hologram mask region. A circular region of 4 µm diameter is first 'milled' onto the top of the Si_3N_4 film by removing the Pt coating using focused ion beam technology. The process is controlled by inspection of the secondary electron microscopy (SEM) image contrast change and stopping the milling at the desired time. Slight over-milling into the Si_3N_4 is often necessary in order to remove any residual Pt islands that could be formed during the Ga^+ milling process, which improves the quality of the phase mask. The computer-generated hologram is then binarized and the pattern transferred on the exposed region of the Si_3N_4 membrane in terms of a two-level thickness variation. The mask thus produced now acts as a phase mask to incoming electron beams. The first column in figure 3 shows the SEM images of those masks designed to imprint the TBB_{01}, TBB_{11} and TBB_{21} modes.
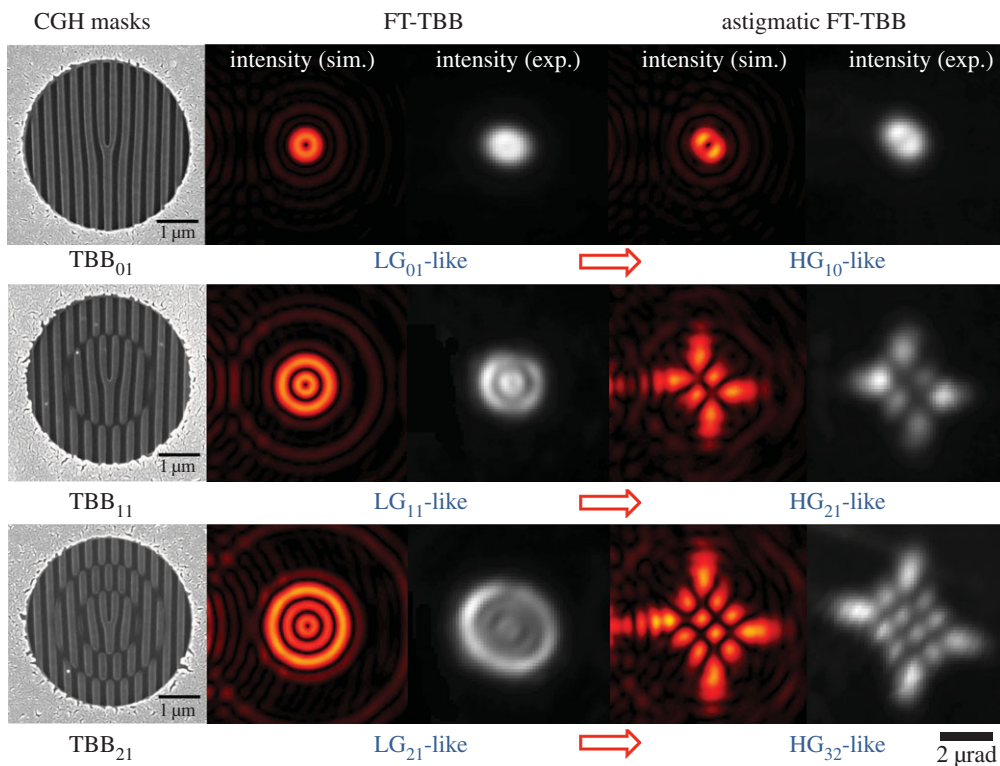
Figure 3. Experimental realization of the radial TBB modes of an electron vortex beam: column 1 (from the left) shows the SEM images of the nano-fabricated CGH masks; column 2 and column 3 are, respectively, the simulation and experimental observation of the intensity distribution of FT-TBB modes at the focal plane of the lens. Columns 4 and 5 are, respectively, the simulation and experimental results of the astigmatic transform of the FT-TBB modes. The rows from top to bottom are for $p = 0$, $p = 1$ and $p = 2$, respectively, each with azimuthal index $l = 1$.

The computer-generated hologram (CGH) phase mask is then placed at the sample plane of the JEOL 2200FS transmission electron microscope (TEM) equipped with a field emission gun, operating at 200 kV. The through-focus images are then obtained in the low-angle diffraction mode. In this mode, the objective lens is switched off and a low convergence angle is used which effectively confers a longer camera length to observe non-overlapping diffracted order beams. A 20 μm diameter selected area aperture is then used to enhance the image contrast by exclusion of stray beams.

The second and third columns in figure 3 present a comparison between the simulation and experimental results for the FT-TBB modes produced at the focal plane of the TEM's magnetic lens. The intense feature within the focused spots shows fine multiple ring features for modes with $p > 0$. In that respect, they are similar to the LG modes of different radial p indices. Unlike the LG modes, FT-TBB modes have additional weak rings (they are more obvious in the pseudo-colour images for the simulated results) that can be attributed to the sharp cut-off of the apertures in the momentum space. These faint ring structures correspond to the side bands of the Airy functions for the non-vortex mode $p = 0$ and $l = 0$. Owing to the presence of these faint rings, it is strictly not correct to apply the simple rule, valid for LG modes, that the radial index can be inferred from the number of dark rings between the bright rings. However, the rule is approximately obeyed if we just focus on the intense part of the FT-TBB modes, as can be seen in the experimental results in the third column of figure 3. A more striking feature of the FT-TBB modes is that the brightest part of the multi-ring structure is located at the outer-most ring. This is in direct contrast with the intensity distribution in the LG modes where the inner-most ring is the

most intense, consistent with the Gaussian character of the intensity envelop of the LG beam. The detailed analysis of these contrasting behaviours will be further discussed in a separate paper.

As explained in the 1992 paper by Allen *et al.* [1], it has been suggested by [36,49] that an appropriate cylindrical lens system can be used to transform HG laser beams with spatial dependence $H_n(x)H_m(y)$ into a single LG mode defined by LG_{pl} or $LG_{m,n-m}$ for $n \geq m$. The reverse is also true and can be used as a means to identify not only the value of l, but also that of p. In a lens system, the cylindrical lens action can be achieved by the appropriate excitation of the stigmator lens. We have applied the same astigmatic mode transformation inside our electron microscope using the electron stigmator. The experimental results of this astigmatic mode transformed beam intensity together with the corresponding simulation results are shown in the last two columns of figure 3. Again, focusing on the intense part of the beam, we can show that the resulting astigmatic mode transformed pattern is HG-like with the radial and azimuthal indices p and l readily read out from the number of dark lines within the patterns.

4. Discussion

Our results show that the normal modes of the electron vortex beams also have LG-like qualities with the number $p + 1$ of 'bright' rings related to the radial index. The analogy to the LG beams can be stretched further to encompass astigmatic transformation. We see that the circular transverse structure of our vortex normal modes has been transformed into rectangular array patterns, in a similar manner to the astigmatic transformation of the LG modes. This similarity has been recognized by Shiloh *et al.* [51] for the $p = 0$ modes, although no explanation was offered until now. However, our result shows that such an analogy is only approximately valid. The presence of the side bands or the outer faint rings in the electron vortex beam case makes the strict application of the LG-based rule to be false. This needs to be taken into consideration when the sideband intensity becomes comparable to the intensity of the central part of the electron vortex beam.

The physical significance of the radial index in optical vortex beams has been the subject of detailed discussions recently [27,34,35,52]. The radial modes can be related to the radial displacement due to the Gouy phase change. The orthogonality of the optical vortex radial modes has been experimentally verified [48]. We envisage that this report on the preparation of radial normal modes in the context of electron vortex beams will stimulate further research with possible applications in quantum technologies. In particular, it may also be a good field-independent quantum basis to explore interesting magnetic field-induced effects on electron vortex beams [53–57].

5. Conclusion

In conclusion, we have given a brief description of the main progress that has been made since 2010 when electron vortex beams were first experimentally demonstrated. This was followed by the description of our recent work concerned with the transverse normal mode structure of coherent electron vortex beams involving the specification of two independent quantum numbers l and p. This natural quantum basis is ideal for electron sources with limited transverse coherence. Experimentally, we have shown that the FT-TBB (electron vortex) can be produced when a fully illuminated circular-apertured TBB-diffractive mask is placed next to the focusing lens. This suggests that we now have full control of the quantum degrees of freedom of the resulting waves. We have verified that the intensity distributions generated experimentally are consistent with the simulation and the topological features as well as the radial structure of the phase wave front have been confirmed by an astigmatic mode transformation analysis. We have emphasized the strong similarities between the transformation described here for electron beams and the astigmatic transformation involving the LG and HG modes in optical beams. The work described here can be regarded as laying the foundations for the quantum manipulation of any matter vortex waves.

References

1. Allen L, Beijersbergen MW, Spreeuw RJC, Woerdman JP. 1992 Orbital angular momentum of light and the transformation of Laguerre–Gaussian laser modes. *Phys. Rev. A* **45**, 8185–8189. (doi:10.1103/PhysRevA.45.8185)

2. Belinfante FJ. 1940 On the current and the density of the electric charge, the energy, the linear momentum and the angular momentum of arbitrary fields. *Physica* **7**, 449–474. (doi:10.1016/S0031-8914(40)90091-X)

3. Humblet J. 1943 Sur le moment d'impulsion d'une onde électromagnétique. *Physica* **10**, 585–603. (doi:10.1016/S0031-8914(43)90626-3)

4. Coullet P, Gil L, Rocca F. 1989 Optical vortices. *Opt. Commun.* **73**, 403–408. (doi:10.1016/0030-4018(89)90180-6)

5. Allen L, Padgett MJ, Babiker M. 1999 IV The orbital angular momentum of light. In *Progress in optics*, vol. 39 (ed. E Wolf), pp. 291–372. London, UK: Institute of Physics. (http://linkinghub.elsevier.com/retrieve/pii/S0079663808703913).

6. Allen L, Barnett SM, Padgett MJ. 2003 *Optical angular momentum*. Bristol, UK: Institute of Physics Publication.

7. Andrews DL, Babiker M. 2012 *The angular momentum of light*. Cambridge, UK: Cambridge University Press.

8. He H, Friese M, Heckenberg N, Rubinsztein-Dunlop H. 1995 Direct observation of transfer of angular momentum to absorptive particles from a laser beam with a phase singularity. *Phys. Rev. Lett.* **75**, 826–829. (doi:10.1103/PhysRevLett.75.826)

9. Dholakia K, Macdonald M, Spalding G. 2002 Optical tweezers: the next generation. *Phys. World* **15**, 31–35. (doi:10.1088/2058-7058/15/10/37)

10. Grier DG. 2003 A revolution in optical manipulation. *Nature* **424**, 810–816. (doi:10.1038/nature01935)

11. Ladavac K, Grier DG. 2004 Microoptomechanical pumps assembled and driven by holographic optical vortex arrays. *Opt. Express* **12**, 1144–1149. (doi:10.1364/OPEX.12.001144)

12. Galajda P, Ormos P. 2001 Complex micromachines produced and driven by light. *Appl. Phys. Lett.* **78**, 249–251. (doi:10.1063/1.1339258)

13. Yao AM, Padgett MJ. 2011 Orbital angular momentum: origins, behavior and applications. *Adv. Opt. Photon.* **204**, 161–204. (doi:10.1364/AOP.3.000161)

14. Fürhapter S, Jesacher A, Bernet S, Ritsch-Marte M. 2005 Spiral interferometry. *Opt. Lett.* **30**, 1953–1955. (doi:10.1364/OL.30.001953)

15. Züchner T, Failla AV, Meixner AJ. 2011 Light microscopy with doughnut modes: a concept to detect, characterize, and manipulate individual nanoobjects. *Angew. Chem.* **50**, 5274–5293.doi:10.1002/anie.201005845)

16. Baranek M, Bouchal Z. 2013 Rotating vortex imaging implemented by a quantized spiral phase modulation. *J. Eur. Opt. Soc.* **8**, 13017. (doi:10.2971/jeos.2013.13017)

17. Bialynicki-Birula I, Bialynicka-Birula Z, Śliwa C. 2000 Motion of vortex lines in quantum mechanics. *Phys. Rev. A* **61**, 032110. (doi:10.1103/PhysRevA.61.032110)

18. Bialynicki-Birula I, Bialynicka-Birula Z. 2001 Motion of vortex lines in nonlinear wave mechanics. *Phys. Rev. A* **65**, 014101. (doi:10.1103/PhysRevA.65.014101)

19. Bialynicki-Birula I, Mloduchowski T, Radozycki T, Śliwa C. 2001 Vortex lines in motion. *Acta Phys. Pol. A* **100 (Suppl.)**, 29–41. (doi:10.12693/APhysPolA.100.29)

20. Bliokh K, Bliokh Y, Savel'ev S, Nori F. 2007 Semiclassical dynamics of electron wave packet states with phase vortices. *Phys. Rev. Lett.* **99**, 190404. (doi:10.1103/PhysRevLett.99.190404)

21. Uchida M, Tonomura A. 2010 Generation of electron beams carrying orbital angular momentum. *Nature* **464**, 737–739. (doi:10.1038/nature08904)

22. Verbeeck J, Tian H, Schattschneider P. 2010 Production and application of electron vortex beams. *Nature* **467**, 301–304. (doi:10.1038/nature09366)
23. McMorran BJ, Agrawal A, Anderson IM, Herzing AA, Lezec HJ, McClelland JJ, Unguris J. 2011 Electron vortex beams with high quanta of orbital angular momentum. *Science* **331**, 192–195. (doi:10.1126/science.1198804)
24. Heckenberg NR, McDuff R, Smith CP, Rubinsztein-Dunlop H, Wegener MJ. 1992 Laser beams with phase singularities. *Opt. Quantum Electron.* **24**, S951–S962. (doi:10.1007/BF01588597)
25. Heckenberg NR, McDuff R, Smith CP, White AG. 1992 Generation of optical phase singularities by computer-generated holograms. *Opt. Lett.* **17**, 221. (doi:10.1364/OL.17.000221)
26. Shiloh R, Lereah Y, Lilach Y, Arie A. 2014 Sculpturing the electron wave function using nanoscale phase masks. *Ultramicroscopy* **144**, 26–31. (doi:10.1016/j.ultramic.2014.04.007)
27. Karimi E, Santamato E. 2012 Radial coherent and intelligent states of paraxial wave equation. *Opt. Lett.* **37**, 2484. (doi:10.1364/OL.37.002484)
28. Béché A, Van Boxem R, Van Tendeloo G, Verbeeck J. 2014 Magnetic monopole field exposed by electrons. *Nat. Phys.* **10**, 26–29. (doi:10.1038/nphys2816)
29. Blackburn AM, Loudon JC. 2014 Vortex beam production and contrast enhancement from a magnetic spiral phase plate. *Ultramicroscopy* **136**, 127–143. (doi:10.1016/j.ultramic.2013.08.009)
30. Yang YJ, Thirunavukkarasu G, Babiker M, Yuan J. Submitted. Principle of chiral rotational symmetry and electron vortex beams.
31. Clark CW, Barankov R, Huber MG, Arif M, Cory DG, Pushin DA. 2015 Controlling neutron orbital angular momentum. *Nature* **525**, 504–506. (doi:10.1038/nature15265)
32. Lembessis VE, Ellinas D, Babiker M, Al-Dossary O. 2014 Atom vortex beams. *Phys. Rev. A* **89**, 053616. (doi:10.1103/PhysRevA.89.053616)
33. Nye JF, Berry MV. 1974 Dislocations in wave trains. *Proc. R. Soc. Lond. A* **336**, 165–190. (doi:10.1098/rspa.1974.0012)
34. Plick WN, Krenn M, Fickler R, Ramelow S, Zeilinger A. 2013 Quantum orbital angular momentum of elliptically symmetric light. *Phys. Rev. A* **87**, 1–9. (doi:10.1103/PhysRevA.87.033806)
35. Harris J, Grillo V, Mafakheri E, Gazzadi GC, Frabboni S, Boyd RW, Karimi E. 2015 Structured quantum waves. *Nat. Phys.* **11**, 629–634. (doi:10.1038/nphys3404)
36. Beijersbergen MW, Allen L, van der Veen HELO, Woerdman JP. 1993 Astigmatic laser mode converters and transfer of orbital angular momentum. *Opt. Commun.* **96**, 123–132. (doi:10.1016/0030-4018(93)90535-D)
37. Juchtmans R, Béché A, Abakumov A, Batuk M, Verbeeck J. 2015 Using electron vortex beams to determine chirality of crystals in transmission electron microscopy. *Phys. Rev. B* **91**, 094112. (doi:10.1103/PhysRevB.91.094112)
38. Lloyd S, Babiker M, Yuan J. 2012 Quantized orbital angular momentum transfer and magnetic dichroism in the interaction of electron vortices with matter. *Phys. Rev. Lett.* **108**, 074802. (doi:10.1103/PhysRevLett.108.074802)
39. Yuan J, Lloyd SM, Babiker M. 2013 Chiral-specific electron-vortex-beam spectroscopy. *Phys. Rev. A* **88**, 031801. (doi:10.1103/PhysRevA.88.031801)
40. Rusz J, Bhowmick S. 2013 Boundaries for efficient use of electron vortex beams to measure magnetic properties. *Phys. Rev. Lett.* **111**, 105504. (doi:10.1103/PhysRevLett.111.105504)
41. Jesacher A, Fürhapter S, Bernet S, Ritsch-Marte M. 2005 Shadow effects in spiral phase contrast microscopy. *Phys. Rev. Lett.* **94**, 233902. (doi:10.1103/PhysRevLett.94.233902)
42. Verbeeck J, Tian H, Van Tendeloo G. 2013 How to manipulate nanoparticles with an electron beam? *Adv. Mater.* **25**, 1114–1117. (doi:10.1002/adma.201204206)
43. Gnanavel T, Yuan J, Babiker M. 2012 Observation of gold nanoparticles movements under sub-10 nm vortex electron beams in an aberration corrected TEM. In *Proc. of the 15th European Microscopy Congress. II.* Manchester, UK: Royal Microscopy Society. See http://www.emc2012.org/documents/Abstracts/Abstracts/EMC2012_1082.pdf.
44. Lloyd SM, Babiker M, Yuan J. 2012 Interaction of electron vortices and optical vortices with matter and processes of orbital angular momentum exchange. *Phys. Rev. A* **86**, 023816. (doi:10.1103/PhysRevA.86.023816)
45. Simpson NB, Dholakia K, Allen L, Padgett MJ. 1997 Mechanical equivalence of spin and orbital angular momentum of light: an optical spanner. *Opt. Lett.* **22**, 52–54. (doi:10.1364/OL.22.000052)

12

rsta.royalsocietypublishing.org *Phil. Trans. R. Soc. A* **375**: 20150438

46. Fetter AL. 2001 Vortices in a trapped dilute Bose–Einstein condensate. *J. Phys. Condens. Matter* **13**, R135–R194. (doi:10.1088/0953-8984/13/12/201)

47. Karimi E, Grillo V, Boyd RW, Santamato E. 2014 Generation of a spin-polarized electron beam by multipole magnetic fields. *Ultramicroscopy* **138**, 22–27. (doi:10.1016/j.ultramic.2013.12.002)

48. Karimi E, Giovannini D, Bolduc E, Bent N, Miatto FM, Padgett MJ, Boyd RW. 2014 Exploring the quantum nature of the radial degree of freedom of a photon via Hong-Ou-Mandel interference. *Phys. Rev. A Atom. Mol. Opt. Phys.* **89**, 1–5. (doi:10.1103/PhysRevA.89.013829)

49. Abramochkin E, Volostnikov V. 1991 Beam transformations and nontransformed beams. *Opt. Commun.* **83**, 123–135. (doi:10.1016/0030-4018(91)90534-K)

50. Schattschneider P, Verbeeck J. 2011 Theory of free electron vortices. *Ultramicroscopy* **111**, 1461–1468. (doi:10.1016/j.ultramic.2011.07.004)

51. Shiloh R, Tsur Y, Remez R, Lereah Y, Malomed BA, Shvedov V, Hnatovsky C, Krolikowski W, Arie A. 2015 Unveiling the orbital angular momentum and acceleration of electron beams. *Phys. Rev. Lett.* **114**, 096102. (doi:10.1103/PhysRevLett.114.096102)

52. Karimi E, Boyd RW, de la Hoz P, de Guise H, Řeháček J, Hradil Z, Aiello A, Leuchs G, Sánchez-Soto LL. 2014 Radial quantum number of Laguerre-Gauss modes. *Phys. Rev. A* **89**, 063813. (doi:10.1103/PhysRevA.89.063813)

53. Greenshields C, Stamps RL, Franke-Arnold S. 2012 Vacuum Faraday effect for electrons. *New J. Phys.* **14**, 103040. (doi:10.1088/1367-2630/14/10/103040)

54. Guzzinati G, Schattschneider P, Bliokh KY, Nori F, Verbeeck J. 2013 Observation of the Larmor and Gouy rotations with electron vortex beams. *Phys. Rev. Lett.* **110**, 093601. (doi:10.1103/PhysRevLett.110.093601)

55. Schattschneider P, Schachinger T, Stöger-Pollach M, Löffler S, Steiger-Thirsfeld A, Bliokh KY, Nori F. 2014 Imaging the dynamics of free-electron Landau states. *Nat. Commun.* **5**, 4586. (doi:10.1038/ncomms5586)

56. Greenshields CR, Stamps RL, Franke-Arnold S, Barnett SM. 2014 Is the angular momentum of an electron conserved in a uniform magnetic field? *Phys. Rev. Lett.* **113**, 240404. (doi:10.1103/PhysRevLett.113.240404)

57. Babiker M, Yuan J, Lembessis VE. 2015 Electron vortex beams subject to static magnetic fields. *Phys. Rev. A* **91**, 013806. (doi:10.1103/PhysRevA.91.013806)